Carnegie Observatories Astrophysics Series, Vol. 4:
Origin and Evolution of the Elements, 2004
ed. A. McWilliam and M. Rauch (Pasadena: Carnegie Observatories,
http://www.ociw.edu/ociw/symposia/series/symposium4/proceedings.html)

New Low- and Intermediate-mass Star Yields: CNO Abundances

M. MOLLÁ[1], M. GAVILÁN[1], and J. F. BUELL[2]
(1)Universidad Autónoma de Madrid, 28049 Cantoblanco, Spain
(2)Department of Physics, Northeastern State University, Tahlequah, OK 74464, USA

Abstract

New stellar yields for low and intermediate mass stars have been calculated taking into account the effects of the convective dredge up and the Hot Bottom Burning (HBB), incorporating the most recent improvements in the TP-AGB processes.

We present the evaluation of these new yields for these stars by using them as input in a Galactic Chemical Evolution (GCE) model. In particular, we analyze if the contribution of these stars is enough to explain the observed behavior of Carbon and Nitrogen vs. Oxygen.

1.1 Introduction

Modern studies (Carigi 2000), Liang 2001) have shown that differences in stellar yields can reflect on appreciable variations in results obtained with a Galaxy Chemical Evolution model (hereafter GCE). One of the reasons for those differences is based in our still bad understanding of the evolution of low and intermediate mass (LIM) stars, mostly in the post main sequence stages, and in the poor knowledge of the influence of the metallicity, mostly by the mass loss by stellar winds, in the evolution of the most massive ones. Thus, in spite of the big effort done for the computation of yields, the matter is not clear at all: any improvement in the stellar evolution theory may have an effect on the value of the yields, and, therefore, on the chemical evolution model results.

One of the most used set of yields for LIM stars has been, historically, this one obtained by Renzini & Voli (1981, hereinafter RV), calculated taking into account the effects of the convective dredge up and the inner layers burning, the so-called *Hot Bottom Burning* (hereinafter HBB), processes. However, these yields are not successful in predicting the observed abundances C/O and N/O. More recently, some other works as Marigo et al. (1996,1998), Van der Hoek & Groenewegen (1997) and Marigo (2001), have treated the evolution of these last phases in this kind of stars, by computing new sets of stellar yields. They, however, show a very different behavior; in particular the metallicity dependence is very different among them (see Marigo 2001). As we have already mentioned, the treatment of the last stages after the main sequence is the most important ingredient in the evolution of these LIM stars, and it is the cause of these dissimilarities.

New yields for LIM stars based in the work performed by Buell (1997) are presented and evaluated in Gavilán, Buell & Mollá (2004). In this piece of work we show the results obtained for a Galactic chemical evolution (hereafter GCE) model when these yields are used in combination with yields from Woosley & Weaver (1995) for massive stars.

1.2 Stellar Structure for LIM Stars during the TP-AGB Phase

The evolution after the main sequence (MS) of stars with masses between 0.8 and 8 $M_\odot$ is determined by the value of their ZAMS mass. This can be divided by the different evolution according to the following mass ranges:

1) 0.8 $M_\odot$ – 1.7 $M_\odot$: The temperatures of the convective shells in these stars does not reach a high enough temperature for CNO reactions to occur, so the composition before and after thermal pulses are the same. They experience a 1st dredge-up event but they do not suffer 2nd or 3rd dredge-up events.

2) 1.7 $M_\odot$ – 4 $M_\odot$: Abundances in these stars are dominated by the 3^{rd} dredge-up, because they suffer many events of this type. The temperature at the base of their envelopes are not high enough to allow CNO reactions, and therefore each dredge-up increases the C and He abundances. The abundance of nitrogen is increased via the second dredge-up.

3) 4 $M_\odot$ – 8 $M_\odot$: The envelope base for 4 $M_\odot$ stars reach a temperature of $30\times10^6 K$, and then the Hot Bottom Burning – a CNO cycle in the base of the envelope– process can take place. The consequence is a decreasing of C and an increasing of N. If there is enough time, it is even possible to convert ^{16}O to ^{14}N, thus producing a decrease of O. The ratio N/O will show a severe increase for stars around 4 $M_\odot$, when the HBB process begin.

The structure of the envelope during the time between thermal pulses is calculated by using a formula to get the luminosity as a function of the stellar mass, the mass of the hydrogen-exhausted core, and the chemical composition The effective temperature of the star is calculated by iterating the temperature until the base of the convective envelope reaches the top of the hydrogen exhausted core.

The changes in abundances of H, He, C, N, and O in the envelope due to nuclear reactions are computed using this structure. Opacities from Rogers & Iglesias (1992) were used when T> 10000 K and the molecular opacities from Alexander & Fergurson (1994) for T< 6000 K. For intermediate values a weighted average of both have been computed. The program used to calculate the LIM star yields follows the surface abundances of H, He, C, N, and O from the first thermal pulse to planetary nebula ejection.

The luminosity of of the low-mass stars on the thermally pulsing asymptotic giant branch (TP-AGB) star starts out at a low value and then grows till it reaches an asymptotic value. This asymptotic value can be expressed as a function of core-mass and the mass of the star and it is modeled using the core-mass-luminosity relations of Boothroyd and Sackmann (1992)

The luminosity is strongly mass dependent for masses over 4$M_\odot$ and determines if a star yields mainly carbon or nitrogen: Stars of lower mass ($M \leq 4M_\odot$) exhibit no hot bottom burning and all of the carbon mixed into the envelope is ejected into the interstellar medium as carbon. Stars of higher mass ($M \geq 4M_\odot$) exhibit very efficient HBB which effectively converts all of the carbon in the envelope into nitrogen until the envelope mass is reduced to a point where HBB is no longer supported.

On the AGB, mass-loss rates are large enough to affect the evolution of the star. This mass-loss prescription is metallicity dependent because the mass-loss rate depends on the radius of the star. Because the radius decreases as metallicity decreases so does the mass-loss rate. This affects the yields by increasing the time a star spends on the TP-AGB allowing for more dredge-up events to occur, increasing the amount of primary production of either carbon or nitrogen. This is essential to understand the evolution of these elements.

Between thermal pulses the base of the convective envelope moves outward in mass by

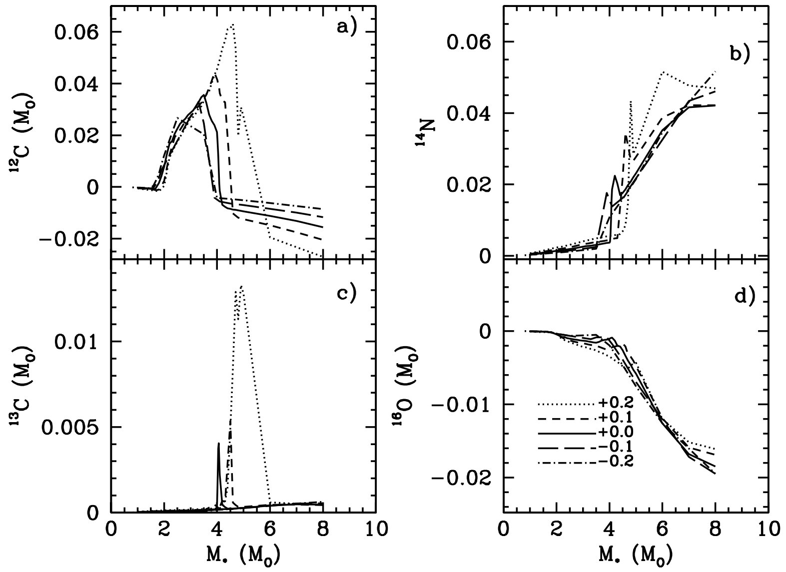

Fig. 1.1. Total yields of ^{12}C, ^{13}C, ^{14}N and ^{16}O produced by LIM stars for different metallicities following label on panel d), expressed as $log(Z/Z_{\odot})$.

an amount ΔM_c and at the end of the succeeding thermal pulse the convective envelope can penetrate into this region and mix these ashes into the envelope of the star. The depth to which the convective zone penetrates is represented by the parameter λ, which is calculated using the formula given in Bazan (1991) $(0 < l < 1)$ $\lambda = 0.90(\log L_{He,max} - \log L_{He,min})$.

Summarizing, the evolution of a LIM star during the TP-AGB phase is dominated mainly by two processes: The third dredge up events and the Hot Bottom Burning (HBB). The first ones affect stars with masses between 2 $M_{\odot}$ and 4 $M_{\odot}$, by increasing the abundance of carbon. In stars more massive than 4 $M_{\odot}$, the HBB produces an abrupt increase of nitrogen and a similar decrease of carbon.

1.3 The New Yields

The resulting stellar yields for ^{12}C, ^{13}C, ^{16}O and ^{14}N as a function of the stellar mass M_*, are shown in Fig 1.1 for 5 values of metallicities: $\log(Z/Z_{\odot})$ = -0.2, -0.1, 0.0, +0.1 and +0.2, and for masses from 1 to 8 $M_{\odot}$.

The proportion primary/total yield is different than in other works. The fraction of the ^{14}N which is primary is shown in Fig. 1.2. The total yield of ^{14}N from solar metallicity stars is comparable to the yield from other metallicities. However, lower metallicity models yield a greater fraction of their ^{14}N as primary yield as opposed to a secondary yield. Lower metallicity stars which experience HBB will produce more primary Nitrogen than the higher metallicity ones. The lower metallicity stars have smaller radii and take longer to reach the superwind phase leaving time for more dredge-up events, meaning more fresh ^{12}C is mixed into the envelope. While HBB is occurring, most of this dredged-up ^{12}C is converted to

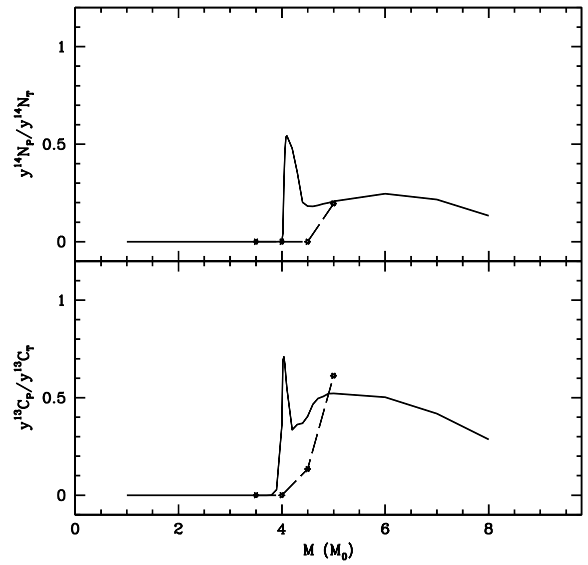

Fig. 1.2. The ratio of the yield of a) primary ^{13}C to the total yield of ^{13}C and b) primary ^{14}N to the total yield of ^{14}N, for solar composition obtained with this new set –solid line– compared with results from Marigo (2001) –dashed line.

primary ^{14}N, resulting in lower metallicity stars producing more primary Nitrogen but less secondary Nitrogen.

These new yields produce less ^{12}C and ^{16}O for $Z = Z_\odot$, when compared with those from RV, M2K and VH, as we can see in Fig.1.3. And they produced more ^{13}C and ^{14}N, than M2K and VH. The described behavior for both elements is different since those authors had not taken into account the transformation from carbon in nitrogen during the HBB phase.

1.4 Multiphase Chemical Evolution Model Description

The model used in this work is the multiphase chemical evolution model (Ferrini et al. 1994; Mollá et al. 1996, 2004). In this model the Galaxy is described as a two-zone system: halo and disk, sliced into cylindrical concentric regions. It takes into account the time evolution of the five populations which inhabit the Milky Way: diffuse gas, molecular clouds, low mass and high mass stars, and stellar remnants.

The gas of the protogalaxy has a mass M(R) computed from the rotation V(R). The gas collapses onto the equatorial plane and forms out the disc. The infall rate is inversely proportional to a characteristic collapse time scale τ_{col}, which changes according to the total mass of the galax which depends on the total mass M(R). Since the mass density depends on galactocentric radius, the collapse time scale also changes along this radius: $\tau_{\rm col} = \tau_{\rm col,0}\exp^{(R/\lambda_D)}$. The rotation curve used for Milky Way Galaxy is calculated from the expression given by Persic, Salucci & Steel (1996) as a Universal Rotation Curve. Parameters Vrot($R_{\rm opt}$), $\tau_{\rm col}$ and λ_D are those corresponding to the radial distribution number 28 of Table 1 from Mollá, Díaz & Ferrini (2004).

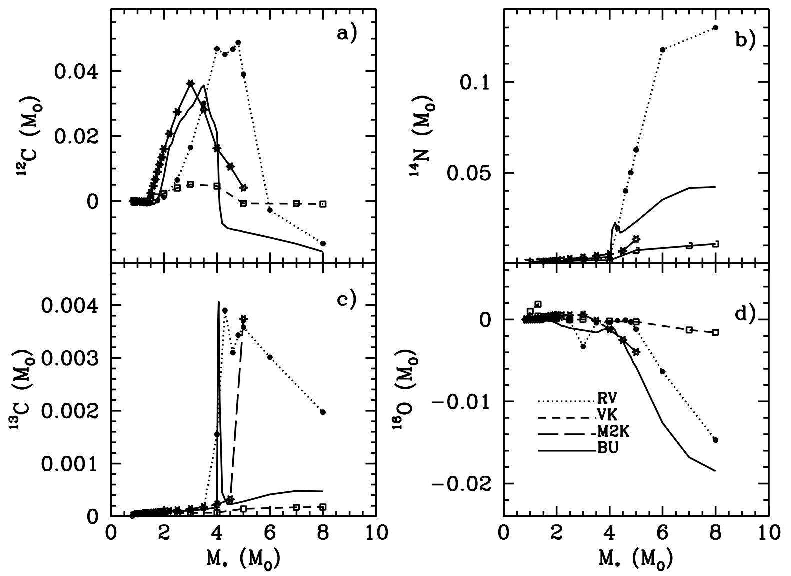

Fig. 1.3. Total yields of ^{12}C, ^{13}C, ^{14}N and ^{16}O produced by LIM stars of solar composition compared with those given by Renzini & Voli (1981), Van der Hoek & Groenewegen (1997) and Marigo (2001), marked with different lines according panel d).

The star formation in the halo, $\mathrm{SFR_H}$, follows a Schmidt law: $\mathrm{SFR_H} \propto \mathrm{Kg}^{1.5}$. Instead that, the star formation law in the disk has 2 steps: 1) molecular clouds c are formed from the diffuse gas $c \propto \mu g^{1.5}$. Stars s form through cloud-cloud collisions: $s \propto Hc^2$. Stars also form from the interaction between massive stars and molecular clouds: $s \propto acs^2$. Parameters K, μ, H and a change along the galactocentric radius through the volume of each region and the efficiency (probability) of each process:

$$K = \epsilon_K (G/V)^{1/2} \tag{1.1}$$

$$\mu = \epsilon_\mu (G/Vd)^{1/2} \tag{1.2}$$

$$H = \epsilon_H Cte/Vd \tag{1.3}$$

$$a = \epsilon_a (Grc)^{1/2} < ms2 > \tag{1.4}$$

The efficiency ϵ_a does not change with R and it is constant for all galaxies (local process). The efficiency ϵ_K is also assumed as constant for all halos. Efficiencies ϵ_μ and ϵ_H are variable for each galaxy. Values used for Milky Way Galaxy are $\epsilon_\mu = 0.45$ and $\epsilon_H = 0.13$.

1.5 Results

1.5.1 Abundances for the Solar Neighborhood and the Galactic Disk

Now we will analyze the results of our GCE model. First, we see if these yields are able to reproduce the interstellar medium, the solar abundances and other young star data. This is shown in Fig.1.4. We have at the left the time evolution of Oxygen, Carbon and

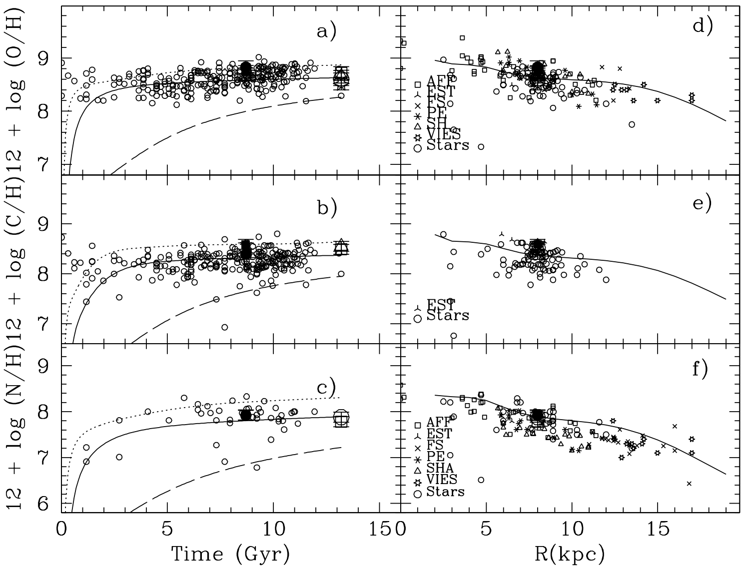

Fig. 1.4. CNO abundances in MWG. Left. Time evolution of Oxygen –a)–, Carbon –b)– and Nitrogen –c), for three regions, inner (4 kpc), solar (8 kpc) and outer (16 kpc), in the disk. Solar abundance values are the large filled symbols by assuming an age of 4.5 Gyr for the sun while empty symbols at 13.2 Gyr are the interstellar medium abundances (see text for references). Right. Radial distributions of these same abundances Oxygen –d)–, Carbon –e)– and Nitrogen –f) at the present time. Data are the stellar abundances (open dots) taken from references given in Gavilán, Buell & Mollá (2004), while the other sets of data shown in right panels refer to HII region abundances from Peimbert (1979)–PE–, Shaver et al. (1983) –SHA–, Fich & Silkey (1991) –FS–, Vilchez & Esteban (1996) –VIES–, Afflerbach, Churchwell, & Werner(1997)–AFF-, and Esteban et al. (1999,1999b,1999c) –EST–, as marked in the figure.

Nitrogen (panels a), b) and c), respectively) for three different region: the inner one at 4 kpc (dotted line), the solar at 8 kpc (solid line) and the outer ones at 16 kpc (long dashed line).

Solar abundance values are the large filled symbols taken from Grevesse & Sauval (1998)–circles–, Holweger (2001)–squares– and Allende-Prieto et al. (2001,2002,2002b),–crosses–, by assuming an age of 4.5 Gyr for the sun. Empty symbols at 13.2 Gyr are the interstellar medium abundances given by Meyer et al. (1997,1998), –circles–, Peimbert (1999) –squares–, Meyer et al. (1997) and Sofia & Meyer(2001), –triangles–, and Moos et al. (2002), –stars. It is clear that using these new yields a GCE model reproduces well both solar and ISM abundances. Moreover they reproduce well the stellar observed data shown by the open dots (see Gavilán, Buell & Mollá 2004 for data references). The time evolution of relative CNO abundances also are well fitted.

All observed radial gradients, shown in right panels for Oxygen –d–), Carbon –e)– and Nitrogen –f)–, seem to be well reproduced taking into account the dispersion of data, too. In this case we represent the stellar data for young objects and we also have included the

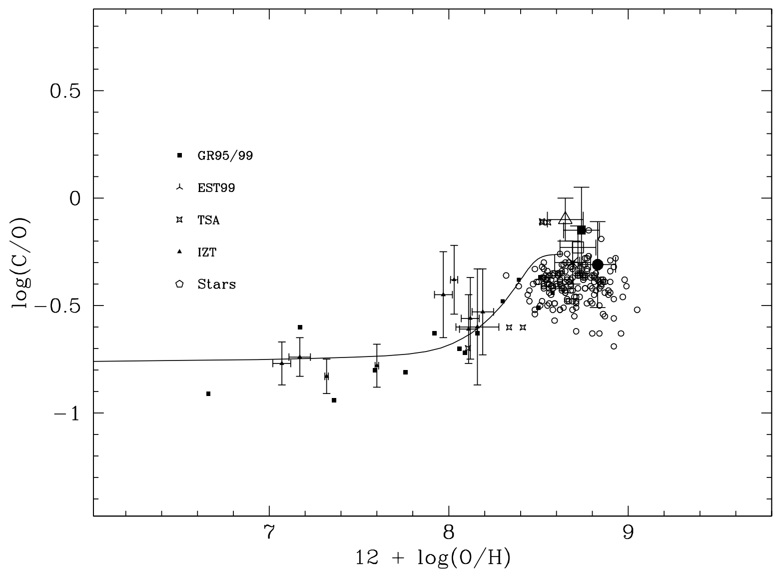

Fig. 1.5. The relative abundance C/O in logarithmic scale *vs* the oxygen abundance 12+ log(O/H) for the Solar Neighborhood. Data are from Esteban et al. (1999,1999b,1999c) –EST99–, and Tsamis et al. (2002), –TSA– for galactic HII regions, from Garnet et al. (1995,1999), for other galaxies HII regions and from Izotov & Thuan (1999) –IZ– for Blue compact dwarf galaxies.

HII region abundances from Peimbert (1979), Shaver et al. (1983), Fich & Silkey (1991), Vilchez & Esteban (1996), Afflerbach et al. (1997), and Esteban et al. (1999).

1.5.2 The Relative Abundances C/O and N/O vs *O/H*

In Fig. 1.5, we represent the relative abundance log(C/O) *vs* the oxygen abundance as 12+log(O/H). This kind of figure is usually difficult to reproduce with chemical evolution models. The question is why two primary elements produced mostly by the same type of stars do not present a flat slope in this diagram. Due to this fact, massive star yields computed with stellar evolution including strong stellar winds in thes stars are invoked to explain the increasing of the relative abundance C/O with increasing O/H. Stellar winds are assumed dependent on metallicity, and therefore, when the abundance increases, more mass is loss from the massive stars. This loss mass has a high abundance in Carbon, and prevents the production of oxygen.

However, we see that this observed increase of C/O is reproduced with the new yields, even using the yields from Woosley & Weaver (1995) for massive stars, where this mass loss by stellar winds is not included. Therefore, the variable slope of C/O vs O/H may be explained with the normal evolution of LIM stars instead of using yields with mass loss for massive stars. This migth imply that the mass loss by stellar winds and its dependence on metallicity may be smoother.

Now, we will analyze the relative abundance log(N/O) *vs* the oxygen abundance as 12+ log(O/H). In this graph, observations of N/O has a slope close to zero at the beginning,

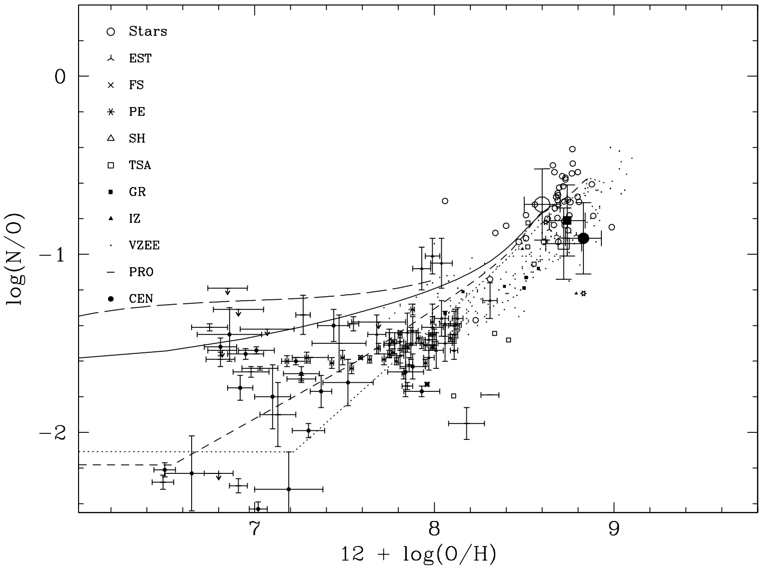

Fig. 1.6. The relative abundances of log (N/O) *vs* the Oxygen abundance as $12+log(O/H)$ for several different radial regions: two inner regions located at 2 and 4 kpc, dotted and short dashed lines, a solar region, solid line, and an outer region, long dashed line, respectively. Stellar abundances are the open dots. Galactic HII regions data are from Peimbert (1979) –PE–, Shaver et al. (1983) –SHA–, Fich & Silkey (1991), –FS–, Esteban et al. (1999,199b,1999c), –EST99–, and Tsamis et al. (2002) –TSA–. Other galaxy data Garnett et al. (1995, 1999) –GR95/99–, Van Zee et al (1998) –VZEE– and Izotov & Thuan (1999) –IZ–are also shown. DLA data from Prochaska et al.(2002) and from the compilation by Centurión et al. (2003) are also included, and represented with error bars. The meaning of symbols is given in the figure

and then develops a positive slope. This change is caused by the ejection of the secondary nitrogen. The flat initial slope, however, implies the existence a primary component of Nitrogen, which migh be produced by the rotation of the stars (Meynet & Maeder, 2002). On the other hand, some authors claimed that different evolutionary rates may also produce this behavior, and, furthermore, are necessary to obtain a dispersion like the observed one.

One of the most interesting result obtained in this work is that the observed behavior, with a flat slope at low metallicities, is naturally obtained. That is, with these new yields we may reproduce the N/O data, as we may see if the Fig.1.6. There, the evolution for the solar region (solid line), shows a very clear primary behavior for the low abundance range, due to the primary nitrogen produced by these new yields for LIM stars, and then N/O increases as observations shown.

Moreover, the ratio of primary to secondary increases for the poor metal stars, and therefore, regions with different evolutionary rates may have different N/O values for a same O/H abundance. Thus, when we represent three other different regions, an outer low evolved region of the disk located at 16 kpc (long dashed line) and two other most evolved regions (short dashed and dotted line) located at 2 and 4 kpc, we see that these last ones show a very different track than the first one. The outer region maintain the flat slope due to the primary component for a larger range of abundances, while the evolved inner regions start in lower values of N/O but increases rapidly, showing a clear secondary behavior even for the lowest O/H abundances. This produces a dispersion in the low abundance regime. Therefore, these yields probably will allow to reproduce all data when all kind of galaxies will be modeled by chemical evolution models.

1.6 Conclusions

LIM star yields used for this work are based on a deep study of the transformations that stars with mass between 0.8 $M_{\odot}$ and 8 $M_{\odot}$ suffer after Main Sequence (Buell 1997), mainly in the TP-AGB, where third dredge up and Hot Bottom Burning events take place. This detailed modeling of the TP-AGB phase basically affects to the production of Nitrogen and Carbon.

We have used these new yields in a model of Chemical Evolution of the Galaxy. The results of the model for our Galaxy, using a combination of these yields for LIM stars with Woosley & Weaver (1995) yields for massive stars, reproduce adequately all kind of abundance observations.

For reproducing the trend of C/O vs O/H, it is not necessary to use yields where the metallicity dependence is due to the mass loss by stellar winds in massive stars. Maybe this mass loss for massive stars is lower than usually assumed.

The trend of N/O vs O/H may be reproduced by the GCM. In particular, our results differ from low-evolved to high-evolved regions. The first one may maintain a flat slope up to reach an oxygen abundances ~ 8. Instead that, the evolved regions begins at a smaller value log(N/O) and then they start to show a secondary behavior at lower metallicities.

We probably might obtain a similar dispersion of that observed in this diagram, when these yields will be included in chemical evolution models applied to low mass dwarf galaxies. The proportion of primary N in these yields, and its dependence on Z seem to be the rigth ones.

References

Afflerbach, A., Churchwell, E., & Werner, M. W. 1997, ApJ, 478, 190
Alexander, D. R. & Ferguson, J. W. 1994, ApJ, 437, 879
Allende Prieto, C., Lambert, D. L., & Asplund, M. 2002, ApJL, 573, L137
Allende Prieto, C., Barklem, P. S., Asplund, M., & Ruiz Cobo, B. 2001, ApJ, 558, 830
Allende Prieto, C., Lambert, D. L., & Asplund, M. 2001, ApJL, 556, L63
Boothroyd, A. I. & Sackmann, I.-J. 1992, ApJL, 393, L21
Bazan, G. 1991, Ph.d Thesis, University of Illinois
Buell, J.F. 1997, Ph.D. Thesis, Univer. of Oklahoma, U.S.A
Carigi, L. 2000, Revista Mexicana de Astronomia y Astrofisica, 36, 171
Centurión, M., Molaro, P., Vladilo, G., Péroux, C., Levshakov, S.A., & D'Odorico, 2003, A&A, 403, 55
Esteban, C., Peimbert, M., Torres-Peimbert, S., & García-Rojas, J. 1999c, Revista Mexicana de Astronomia y Astrofisica, 35, 65
Esteban, C., Peimbert, M., & Torres-Peimbert, S. 1999b, A&A, 342, L37
Esteban, C., Peimbert, M., Torres-Peimbert, S., García-Rojas, J., & Rodríguez, M. 1999a, ApJS, 120, 113
Ferrini, F., Mollá, M., Pardi, M. C., & Diaz, A. I. 1994, ApJ, 427, 745
Fich, M. & Silkey, M. 1991, ApJ, 366, 107
Garnett, D. R., Skillman, E. D., Dufour, R. J., Peimbert, M., Torres-Peimbert, S., Terlevich, R., Terlevich, E., & Shields, G. A. 1995, ApJ, 443, 64
Garnett, D. R., Shields, G. A., Peimbert, M., Torres-Peimbert, S., Skillman, E. D., Dufour, R. J., Terlevich, E. & Terlevich, R. J. 1999, ApJ, 513, 168

Gavilán, M., Buell, J. F. & Mollá, M. 2004, A&A, submitted
Grevesse, N. & Sauval, A. J. 1998, Space Science Reviews, 85, 161
Holweger, H. 2001, AIP Conf. Proc. 598: Joint SOHO/ACE workshop "Solar and Galactic Composition", 23
Izotov, Y. I. & Thuan, T. X. 1999, ApJ, 511, 639
Liang, Y.C., Zhao, G. & Shi, J.R. 2001, A&A, 374, 936
Marigo, P., Bressan, A. & Chiosi, C. 1996, A&A, 313, 545
Marigo, P., Bressan, A., & Chiosi, C. 1998, A&A, 331,
Marigo, P. 2001, A&A, 370, 194
Meyer, D. M., Jura, M., & Cardelli, J. A. 1998, ApJ, 493, 222
Meyer, D. M., Cardelli, J. A., & Sofia, U. J. 1997, ApJL, 490, L10
Meynet, G. & Maeder, A. 2002, A&A, 381, L25
Mollá, M., Díaz, A. I., & Ferrini, F. 2004, ApJ, submitted
Mollá, M., Ferrini, F., Díaz, A. I. 1996, ApJ, 466, 668
Moos, H. W. et al. 2002, ApJS, 140, 3
Peimbert, M. 1979, IAU Symp. 84: The Large-Scale Characteristics of the Galaxy, 84, 307
Peimbert, M. 1999, Chemical Evolution from Zero to High Redshift , 30
Persic, M., Salucci, P. & Steel, F. 1996, MNRAS, 281, 27
Prochaska, J. X., Henry, R. B. C., O'Meara, J. M., Tytler, D., Wolfe, A. M., Kirkman, D., Lubin, D., & Suzuki, N. 2002, PASP, 114, 933
Renzini, A., & Voli, M. 1981, A&A, 94, 175
Rogers, F.J. and Iglesias, C.A. 1992, ApJS, 79, 507
Shaver, P. A.,McGee, R. X., Newton, L. M., Danks, A. C., & Pottasch, S. R. 1983, MNRAS, 204, 53
Sofia, U. J. & Meyer, D. M. 2001, ApJl, 554, L221
Tsamis, Y.G., Barlow, M.J., Liu, X.-W., Danzinger, I.J. & Storey, P.J. 2002, astro-ph/0209534
Van den Hoek, L. B. & Groenewegen, M. A. T. 1997, A&AS, 123, 395 (VG)
van Zee, L., Salzer, J.J., Haynes, M.P., O'Donoghue, A.A., Balonek, T.J., 1998, AJ, 116, 2805
Vílchez, J. M. & Esteban, C. 1996, MNRAS, 280, 720
Woosley, S. E. & Weaver, T. A. 1995, ApJS, 101, 181 (WW)